

## **Development of Digital Twin Replicas for Computational Analysis of Nonwoven Nanofibrous Air Filter Media**

Ivan P. Beckman<sup>1,2</sup>, Gentry Berry,<sup>1</sup> Heejin Cho,<sup>1</sup> and Guillermo Riveros<sup>2</sup>

<sup>1</sup>Institute for Clean Energy Technology, 205 Research Blvd, Mississippi State, MS 39759, USA

<sup>2</sup>U.S. Army Engineer Research and Development Center, Vicksburg, MS 39180, USA

### **ABSTRACT**

Recent advances in high performance computing and general availability of computational fluid dynamics software have greatly increased the viability of computational modeling of air filtration as a complement to both analytical and experimental models. Computational air filtration models require realistic digital geometry—a digital twin of actual filter media. While the structure of non-woven nanofibrous air filtration media can be observed with a microscope, the replication of media characteristics such as fiber diameter, filter thickness, and solidity are difficult to estimate. Current research at Mississippi State University and the US Army Engineer Research and Development Center has led to the development of techniques and algorithms to produce digital twin geometry with uniform random fiber alignment and tunable parameters that replicate typical air filtration media for use with computational fluid dynamics software such as Ansys Fluent. An effective digital twin geometry can be adjusted for fiber stiffness, spacing, and shape and can incorporate particle loading. By incorporating analytical calculations from the Single Fiber Efficiency model, digital twin air filter media can enable the prediction of filtration efficiency and air flow resistance in the design of new filter materials. Digital twin replicas of air filter media also enable the prediction filtration efficiency and air flow resistance through machine learning algorithms using a convolutional neural network to assess filter media characteristics.

### **INTRODUCTION**

Air filtration research began in earnest in the early 1940s during the Second World War [1], [2]. Key research by the U.S. Army Chemical Warfare Service Laboratory and the Naval Research Laboratory led to the development of CWS Type 6 filter paper used in collective protector filter units [1]. Originally manufactured from a combination of cellulose and asbestos fibers, the CWS Type 6 paper was later adopted by the Atomic Energy Commission as the precursor to modern day High Efficiency Particulate Air (HEPA) filters [1]. The U.S. Department of Energy (DOE) has long recognized the importance of air filtration research [3]–[7]. The DOE tests and installs modern day HEPA filters for nuclear power, research, and waste containment facilities as a final line of defense to capture hazardous aerosol particles. The Institute for Clean Energy Technology at Mississippi State University recently developed a Nuclear Quality Assurance (NQA-1) program for the advancement of nuclear air cleaning and treatment [8]–[10]. While experimental research of air filtration began in the 1940s, analytical theory of air filtration followed in the 1950s with the work of Nobel Laureate Irving Langmuir [1]. His theory was advanced by many scientists and researchers who collectively developed the single fiber efficiency (SFE) model consolidated by the works of Davies, Brown, and Hinds [11]–[13]. As a complement to experimental and analytical modeling of air filtration, recent advances in high performance computing technology have enabled the advancement of computational models. The U.S. Army

Engineer Research and Development Center Information Technology Laboratory (ERDC-ITL) manages the Department of Defense High Performance Computing Modernization Program. ERDC-ITL conducts research and development for the integration of computational modeling to complement experimental and analytical modeling of challenging problems. The development of digital twin air filter geometry enables a holistic approach to air filtration research by integrating computational modeling and machine learning techniques into analytical and experimental research.

## METHODS

### Digital Twin Replica of Air Filter Media

A digital twin is simply a numerical representation of a physical object, with digital twins of air filter media enabling analytical and computational analysis of their physical counterparts. Creation of digital twin filter media begins by considering the real physical process involved in creating the filter media. Whether dry-laid, wet-laid, melt-blown, or electrospun, fibers are individually laid on top of each other with random orientation, resting on and conforming to the shape of previously laid fibers. An algorithm to create a digital twin begins with this physical process in mind by using a square frame to contain the fibers while also allowing the fibers to terminate inside the square, create additional spacing between fibers and vary the fiber sizes and flexibility [14]. Input parameters are specified, output parameters are produced by the model, and design parameters determine when the model is complete. Table I lists possible input, design, and output parameters of a digital twin algorithm.

Table I. Input, Process, Design, and Output Parameters

Symbol	Type	Description
$L$	Input Parameter	Length of square side dimension
ends	Input Parameter	Percentage of fibers that terminate (broken fibers)
maxslope	Input Parameter	Flexibility of the fibers
$d_f$	Input Parameter	Fiber diameter (fixed or random distribution)
spacing	Input Parameter	Spacing or gaps between fibers
$T, U_0, \rho_g$	Input Parameter	Air temperature, air velocity, air density
$d_p, \rho_p$	Input Parameter	Particle diameter, particle density
$\alpha$	Output Parameter	Solidity or solid volume fraction of fibers
$t$	Design or Output	Thickness of the filter media
$E_f$	Design or Output	Total filter efficiency of the filter media
FC	Design or Output	Face coverage (projection of fiber profiles onto base plane)
$\Delta P$	Design or Output	Air flow resistance (pressure drop across filter)

### Fiber Placement Algorithm

The  $x$ - $y$  plane can be considered as the top surface of a table with each fiber individually dropped onto the table by gravity. To begin, a random orientation of the fiber centerline is determined as shown in Figures 1(a) and 1(b), which illustrate two methods of random selection for the orientation. Figure 1(a) shows two points along the square selected as fiber centerline endpoints, whereas Figure 1(b) shows a random internal angle and distance from the center of

the square to a point on the fiber centerline. Several other methods for selecting a random fiber centerline orientation include selecting random points inside the square, selecting random angles of elevation, and combinations of different methods. Glass HEPA filter media typically has fibers that terminate with their ends inside the square, which can be achieved by selecting random points within filter media along a fiber’s centerline as locations for a break, allowing for termination within the square.

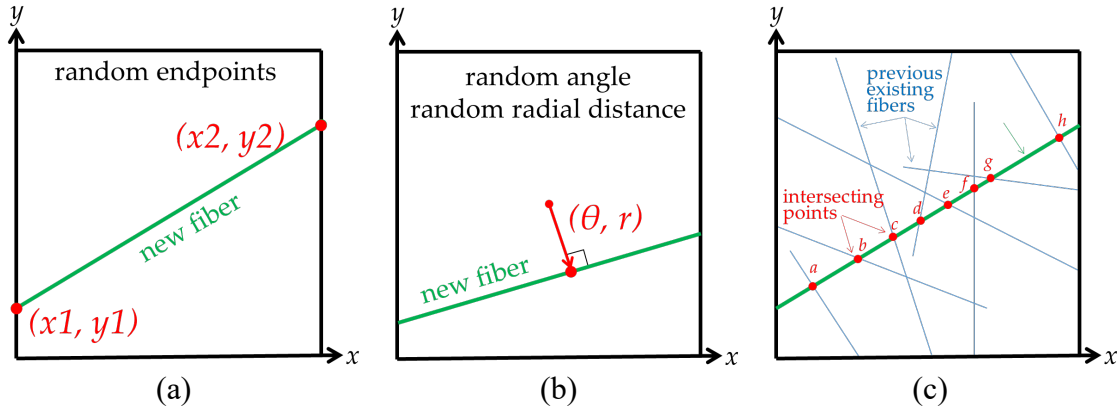


Figure 1. Methods of random fiber orientation in a plane. (a) Selection of two random endpoints along the perimeter of the square. (b) Selection of a random interior point and random angle of elevation. (c) Intersecting points of previous fibers with new fiber [14].

Once the endpoints of the fiber centerline are determined, the centerline is projected onto the  $x$ - $y$  plane along with the centerlines of all previous fibers. The  $(x,y)$  coordinates are determined for the intersection points of the new fiber with previous fibers, as illustrated with points a through h in the example shown in Figure 1(c). These points are potential resting points for the new fiber. The  $z$  coordinates, or height of each point above the table, are calculated from the height of the previous fiber at each particular intersecting point.

Figure 2 rotates the  $y$ -axis from Figure 1 into the table to view from the side  $x$ - $z$  plane. As the new fiber descends onto the nonwoven mesh of previous fibers, it first makes contact with the highest intersecting point, illustrated as point c in the example. The flexibility of the fiber is an input parameter that determines the maximum downward slope from both sides of the highest point, shown as the green dashed line in Figure 2(a). All potential intersecting points that fall below this maximum slope line are eliminated. In the example, points b, d, and e fall below the maximum slope line of Figure 2(a). The new fiber line then descends to the next highest remaining potential intersecting point, shown as point g in the example. Again, the maximum downward slope is considered from this point, and all points below the slope line are eliminated. In the example, point f is eliminated. Figure 2(b) illustrates the remaining four points upon which the new fiber will rest where the break points for each segment are calculated using the intersection of the maximum slope lines. Figure 2(c) illustrates what a new fiber profile would look like, given the step outlined in Figures 2(a) and 2(b). The  $z$  coordinates of the new fiber segments are elevated by the radius of the previous fiber plus the radius of the new fiber and any additional spacing specified by an input parameter. Each fiber segment is recorded into a text file as endpoint coordinates and radii.

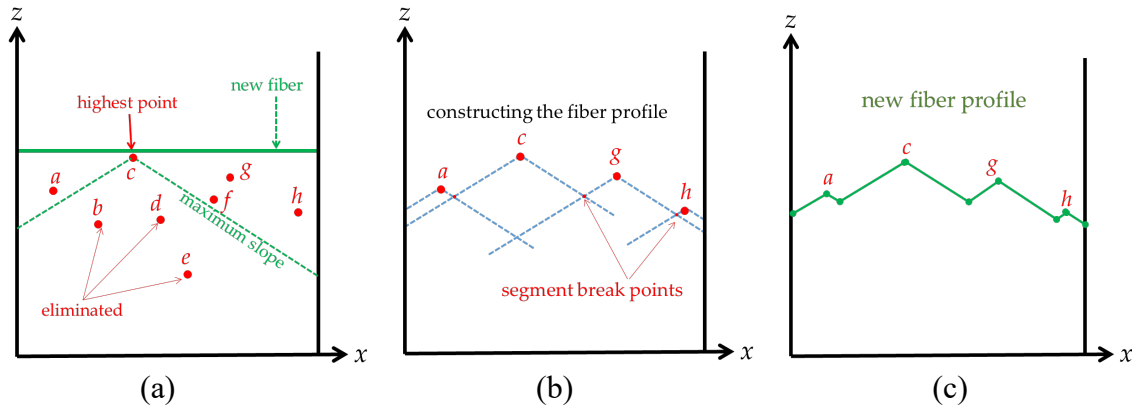


Figure 2. Three methods of random fiber orientation in a plane. (a) Selection of two random endpoints along the perimeter of the square. (b) Selection of a random interior point and random angle of elevation. (c) Fiber normal to random angle and radial distance from center [14].

### Geometry Creation with Ansys SpaceClaim

The text file of fiber segments produced by the Python script is imported into Ansys SpaceClaim and constructed into digital geometry using the SpaceClaim scripting feature. The script reads each fiber segment line, constructs cylinders using the centerline endpoints, and constructs joints between the segments using a sphere of the same radius as the cylinder at the segment endpoints. Figure 3 illustrates the placement of fiber segments with a slope of 15% flexibility laid on top of previous fibers. The orange segment between the two green segments in Figure 3(a) was created with by inserting a sphere where the endpoints join to ensure a smooth transition without gaps.

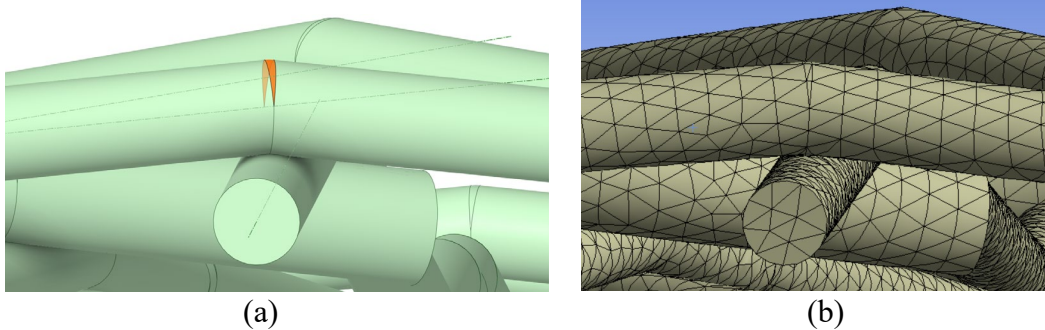


Figure 3. Example of geometry construction. (a) New fibers placed on previous fibers with 15% slope. (b) Meshing of the geometry with Ansys Mechanical [14].

### Single Fiber Efficiency Model

The SFE model may be used to provide a linkage between analytical and computational models. The SFE model considers the efficiency and flow resistance of a single fiber placed normal to the direction of air flow as shown by Figure 4. Of the geometrically incident particles that approach the fiber, the single fiber efficiency  $E_{\Sigma}$  is the percentage of particles that collide with and attach to the fiber. Particle collection mechanisms in the SFE model include collection by interception ( $E_R$ ), diffusion ( $E_D$ ), inertial impaction ( $E_I$ ), and interception of diffusing particles ( $E_{DR}$ ), as illustrated in Figure 4 and shown below in Equations 3–6.

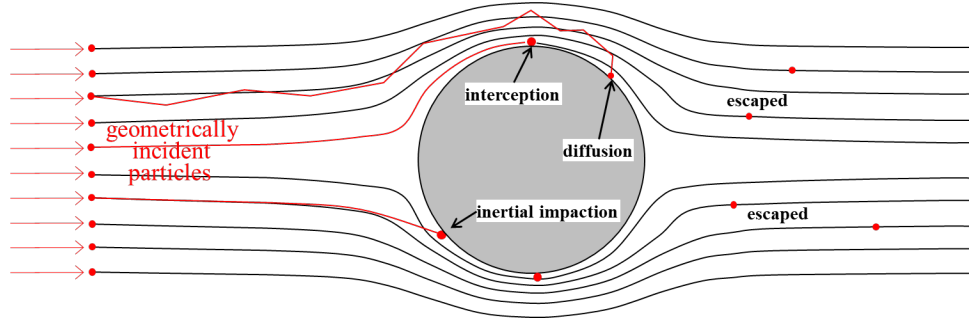


Figure 4. Single Fiber Efficiency model.

The single fiber efficiency  $E_{\Sigma}$  is determined from the collection mechanisms as shown in Equation 2, while the total filter efficiency  $E_F$  is calculated using Equation 1. The air flow resistance, also known as the pressure drop across the filter media, is given as  $\Delta P$  in Equation 7.

$$E_F = 1 - \exp\left(\frac{-4\alpha E_{\Sigma} t}{\pi d_f}\right) \quad (1)$$

$$E_{\Sigma} = 1 - (1 - E_R)(1 - E_D)(1 - E_{DR})(1 - E_I) \quad (2)$$

$$E_R = \frac{(1 - \alpha_f)R^2}{(Ku)(1 + R)} \quad (3)$$

$$E_I = \frac{(Stk)}{2(Ku)^2} [(29.6 - 28\alpha_f^{0.62})R^2 - 27.5R^{2.8}] \quad (4)$$

$$E_D = 2 \cdot Pe^{-2/3} \quad (5)$$

$$E_{DR} = \frac{1.24R^{2/3}}{(Ku \cdot Pe)^{1/2}} \quad (6)$$

$$\Delta P = \frac{\eta t U_0}{d_f^2} [64\alpha_f^{1.5}(1 + 56\alpha_f^3)] \quad (7)$$

For equations 1 through 7,  $t$  is the filter media thickness,  $d_f$  is the fiber diameter,  $\alpha_f$  is the solidity,  $Ku$  is the Kuwabara number,  $R$  is the ratio of particle radius to fiber radius,  $Stk$  is the Stokes number,  $Pe$  is the Peclet number,  $\eta$  is the air viscosity, and  $U_0$  is the air flow velocity. There are many alternative equations for the SFE model present throughout the literature [11]–[13].

### Digital Twin Replica of HEPA Filter Media

By definition, HEPA filters are required to maintain 99.97% filtration efficiency for 300 nm diameter particles with a maximum flow resistance of 320 Pa at ambient conditions with air velocity of 2.5 cm/s [15]. Using the minimum efficiency as a design parameter for a  $20 \mu\text{m} \times 20 \mu\text{m}$  digital twin with 500 nm diameter fibers, the digital twin resulted in 387 fibers with 4,196 segments. The SFE analytical model for this digital twin indicated a flow resistance of 241.8 Pa, which is below the maximum allowable pressure drop. The input, design, and output parameters are given in Table II, and the resulting digital twin geometry is shown in Figure 5.

Table II. Input, Design, and Output Parameters for HEPA Digital Twin

Symbol	Type	Parameter	Description
$d_f$	Input	500 nm	Fiber diameter (fixed or random distribution)
$E_f$	Design	99.97%	Total filter efficiency of the filter media
$\alpha$	Output	18.9%	Solidity or solid volume fraction of fibers
$t$	Output	18.43 $\mu\text{m}$	Thickness of the filter media
FC	Output	8.50	Face coverage
$\Delta P$	Output	241.8 Pa	Air flow resistance (pressure drop across filter)

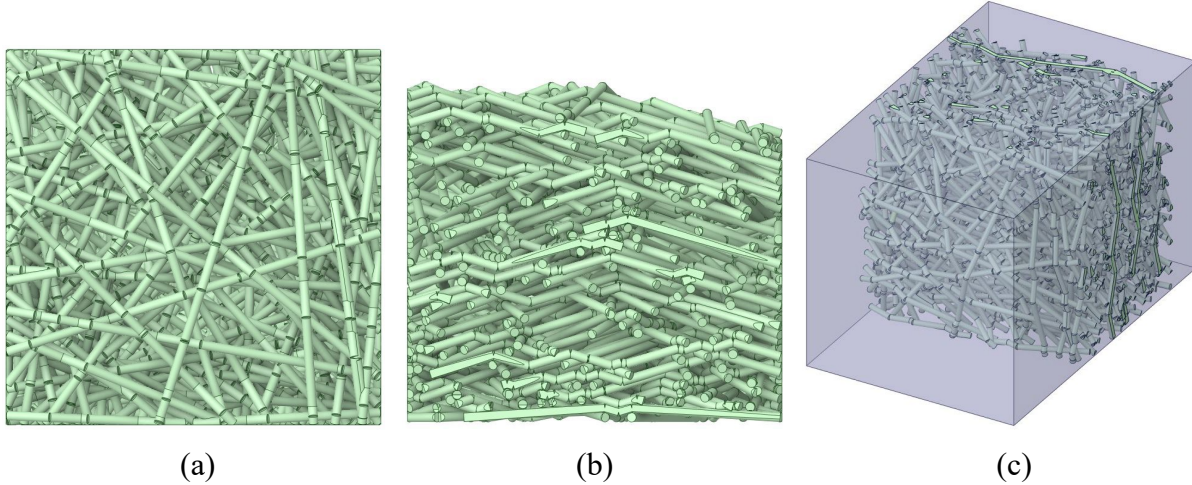


Figure 5. Digital twin of HEPA filter media. (a) Face view,  $20 \mu\text{m} \times 20 \mu\text{m}$ . (b) Profile view showing fibers placed with 30% slope. (c) Digital twin loaded into enclosure for CFD analysis.

The visual representation of HEPA filter media in Figure 5 is useful in understanding the characteristics of actual HEPA media by providing a visualization of different input parameters, such as the effects of fiber flexibility. According to the SFE model, this digital twin achieves 99.97% filtration efficiency with a thickness of 18.43  $\mu\text{m}$  and expected flow resistance of 241.8 Pa. The digital twin can be tuned to match real media by adjusting the input parameters.

## RESULTS AND DISCUSSION

### Computational Fluid Dynamics (CFD) Analysis with Ansys Fluent

The digital twin geometry enables a comparison of the flow resistance obtained using the SFE model with that obtained by using the computational model. Ansys Fluent is useful in evaluating the digital twin with CFD as illustrated in Figure 6, showing three example digital twins, with air flowing from right to left. The red flow within the model near the inlet indicates areas of higher pressure, while the blue flowlines near the outlet indicate lower pressure. Table III compares the flow resistance calculated using the SFE model and results from the CFD model for the three examples. For a simple  $10 \mu\text{m} \times 10 \mu\text{m}$  digital model, the CFD results significantly underestimate the flow resistance compared to that of the SFE model. The computational results come closer to anticipated analytical results with increasing complexity of the digital twin. Additional effort is needed to tune the parameters of the digital twin models in order to achieve a closer correlation of results.

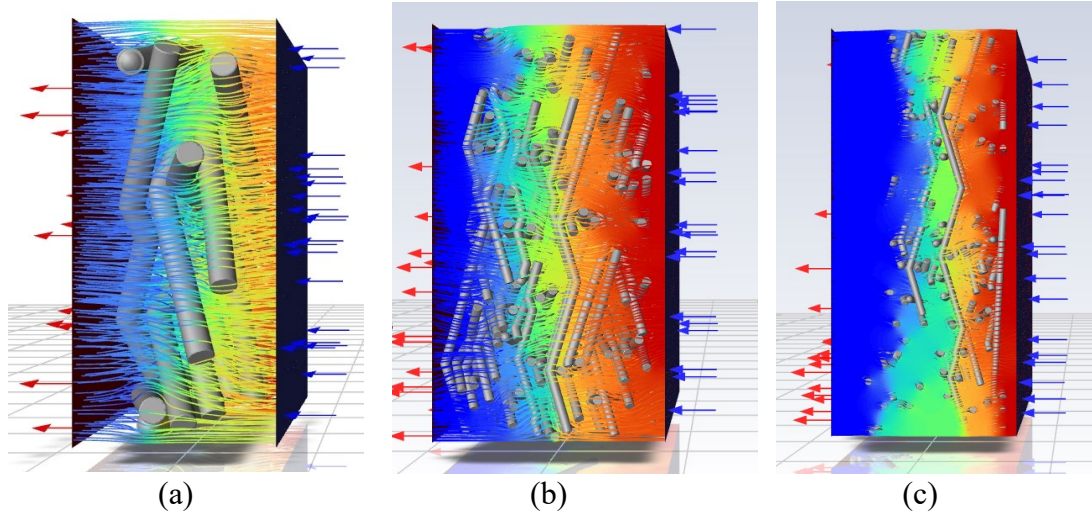


Figure 6. Computational Fluid Dynamics modeling of digital twin filter media.

Table III. Input, Design, and Output Parameters for HEPA Digital Twin

Size	Analytical (SFE) (Pa)	Computational (CFD) (Pa)	Accuracy (%)
10 $\mu\text{m} \times 10 \mu\text{m}$	16.89	5.30	31.4
30 $\mu\text{m} \times 30 \mu\text{m}$	36.7	20.21	55.1
40 $\mu\text{m} \times 40 \mu\text{m}$	34.2	31.11	91.0

### Effects of Particle Loading

The digital twin replica air filter geometry is also useful for studying the effects of particle loading. In the example below, particles are randomly dropped onto the fiber geometry and considered as attached to the fibers upon contact. This can be done for a specified number of particles or until the solidity of the filter increases to a specified level. Figure 7(a) shows a small 10  $\mu\text{m} \times 10 \mu\text{m}$  filter segment with 33 fibers, each 700 nm diameter, a filter thickness of 7.12  $\mu\text{m}$ , and solidity of 16.4%. The SFE analytical model indicated the filter media obtained a total filter efficiency of 69.2% with a pressure drop of 35.0 Pa. The computational analysis of the digital twin in Ansys Fluent indicated a pressure drop of 6.94 Pa between the inlet and outlet planes. As expected, the CFD model significantly underestimated the analytical results at the small scale for a 10  $\mu\text{m} \times 10 \mu\text{m}$  digital twin.

In order to observe the effects of particle loading, random particles were added to the filter until the solidity increased by 10%, from 16.4% to 18.04% as shown in Figure 7(b). A total of 5,957 particles attached to the fibers in a uniform distribution of diameter sizes from 0.1  $\mu\text{m}$  to 0.2  $\mu\text{m}$ . By adjusting the solidity in the analytical SFE model and maintaining constant fiber diameter size and filter media thickness, the analytical SFE model estimates the pressure drop at 43.1 Pa, which is an increase of 23% pressure. The computational model in Figure 7(c) indicates a pressure differential of 9.53 Pa, which is a 37% increase in pressure within the computational model from the clean filter condition.

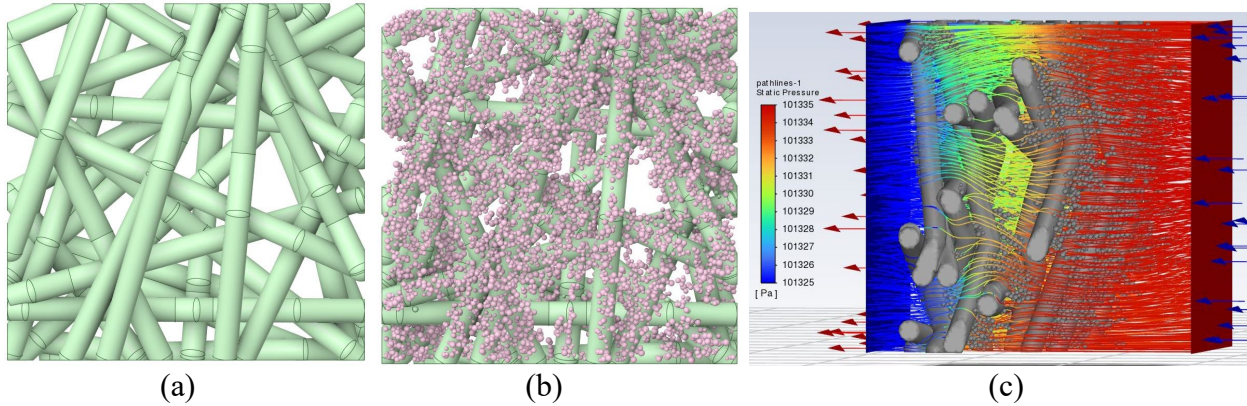


Figure 7. Particle loading analysis of digital twin geometry. (a) Clean digital twin of  $10\ \mu\text{m} \times 10\ \mu\text{m}$  filter. (b) Media loaded with 5957 particles. (c) CFD analysis of the digital twin.

### Digital Twin Comparison with SEM Imagery

The creation of a digital twin geometry enables a visual comparison with physical air filtration media. Figure 8(a) shows a  $10\ \mu\text{m} \times 10\ \mu\text{m}$  SEM image of electrospun and stabilized polyacrylonitrile (PAN) fibers intended for air filtration. Although the fiber diameters are relatively simple to estimate, the resulting solidity and thickness of the media is difficult to determine. The purpose of matching a digital twin geometry to the SEM image is to derive information from the digital twin useful in understanding the air filtration characteristics of the real filter media. Through visual comparison with human eyes, the parameters of the digital twin filter media can be tuned to more closely match the real air filter media and evaluated through the analytical SFE model or computational CFD model.

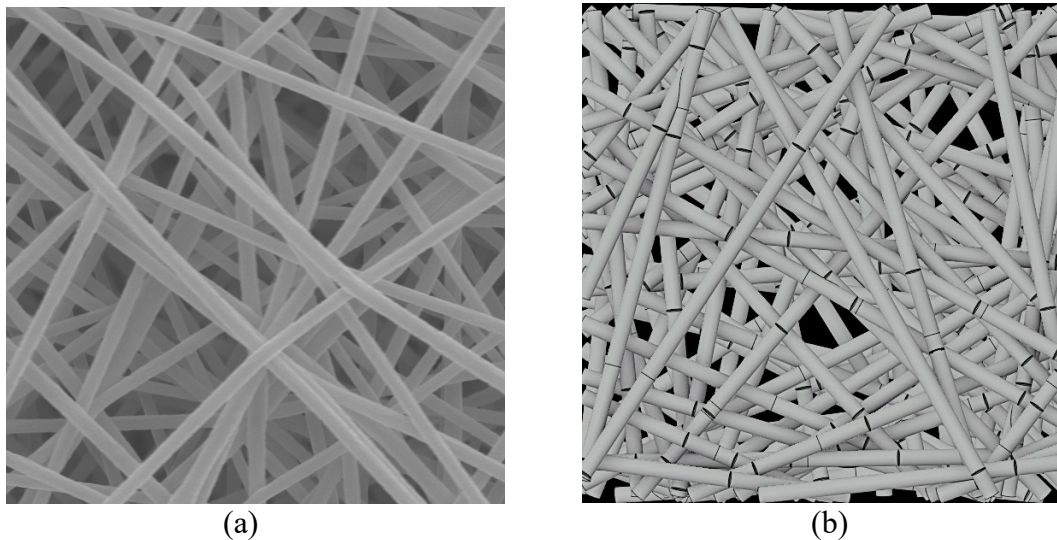


Figure 8. Comparison of electrospun polyacrylonitrile fibers with a digital twin.

Figure 8(b) shows a  $10\ \mu\text{m} \times 10\ \mu\text{m}$  digital twin with 101 fibers created from 454 segments. The fiber diameters are 335 nm, the media thickness is  $7.85\ \mu\text{m}$ , and the solidity is 10.20%. The analytical SFE model indicated the media has a total filter efficiency of 93.2% with air flow resistance of 70.1 Pa.

The digital twin can also be evaluated with a computational model as described above. Figure 9(a) shows the digital mesh, while Figure 9(b) shows the results of CFD analysis using Ansys Fluent with air flow from right to left. The blue air outlet on the left side of the filter was set to 101,325 Pa, while the pressure at the red inlet on the right side was measured as 101,338 Pa. The small scale of the digital twin might contribute to the substantial difference between the analytical and computational estimations of pressure drop across the filter, as discussed in the sections above. Significant effort is required to tune the parameters of the analytical and computational models to achieve a closer correlation of results.

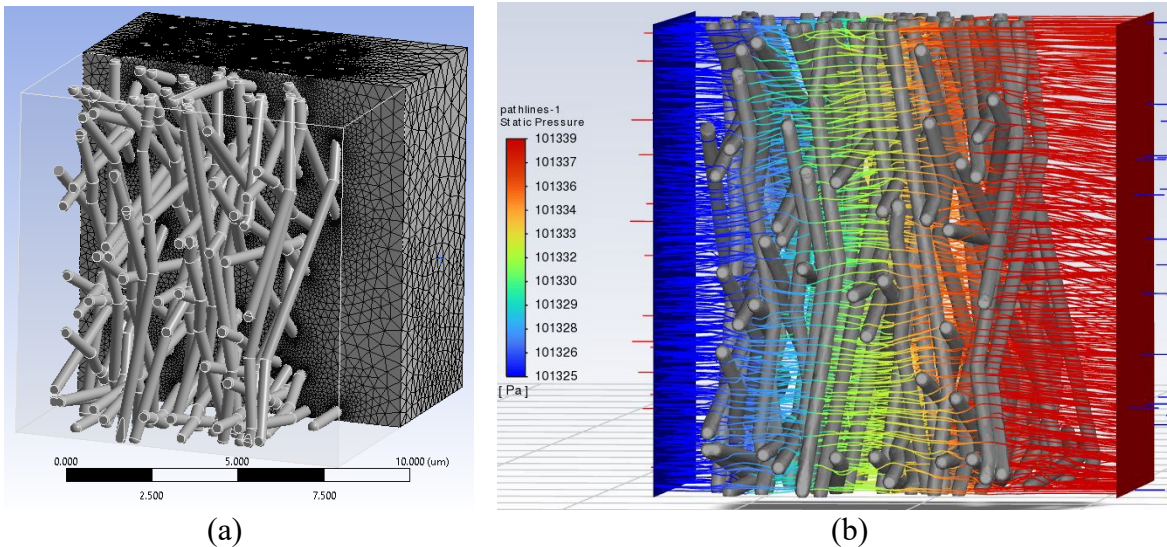


Figure 9. Computational analysis of a digital twin with Ansys Fluent. (a) Digital twin meshing with Ansys Mechanical. (b) Air flow streamlines showing pressure drop across the filter media.

The method of visually observing and comparing digital twin air filter media with SEM images of real media can be assisted by machine learning techniques, specifically convolutional neural networks (CNNs).

### Machine Learning Using a Convolutional Neural Network

A CNN can be trained to evaluate images of digital twin geometry to predict air flow resistance and filtration efficiency as shown by the flowchart in Figure 10. The input and design parameters are fed into the digital twin algorithm, producing a uniform distribution of nonwoven fibers. The algorithm generates a text file of fiber segment endpoints and calculates the filtration efficiency and flow resistance using the SFE analytical model.

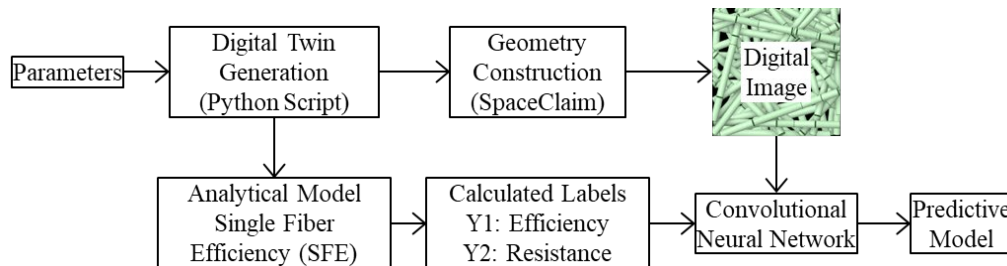


Figure 10. Flowchart for Convolutional Neural Network predictive model.

The digital image is then fed into the CNN as an input, and the efficiency and flow resistance are fed into the CNN as labels. Using a constant  $10\ \mu\text{m} \times 10\ \mu\text{m}$  dimension, ten thousand digital twins were produced using the input parameters described in Table IV. Face coverage was used as the design parameter, while the fiber diameter was varied randomly from 200 nm to 600 nm. The resulting images were tagged with labels for efficiency and resistance.

Table IV. Parameters for CNN Predictive Modeling.

Symbol	Type	Parameter	Description
FC	Design	1.0–3.0	Face coverage (uniform distribution)
$d_f$	Input	200 nm–600 nm	Fiber diameter (uniform distribution)
maxslope	Input	0.15	Fiber flexibility (fixed)
spacing	Input	1.0	No additional spacing between fibers
$E_f$	Output	38.9%–98.7%	Total filter efficiency
$\alpha$	Output	6.58%–21.2%	Solidity or solid volume fraction of fibers
$t$	Output	1.65 $\mu\text{m}$ –11.58 $\mu\text{m}$	Thickness of the filter media
$\Delta P$	Output	13.4–116.7 Pa	Air flow resistance (pressure drop)

The first three images are shown in Figure 11 as examples of ten thousand images produced to train the CNN. Table V shows the associated input parameters and output data for the images.

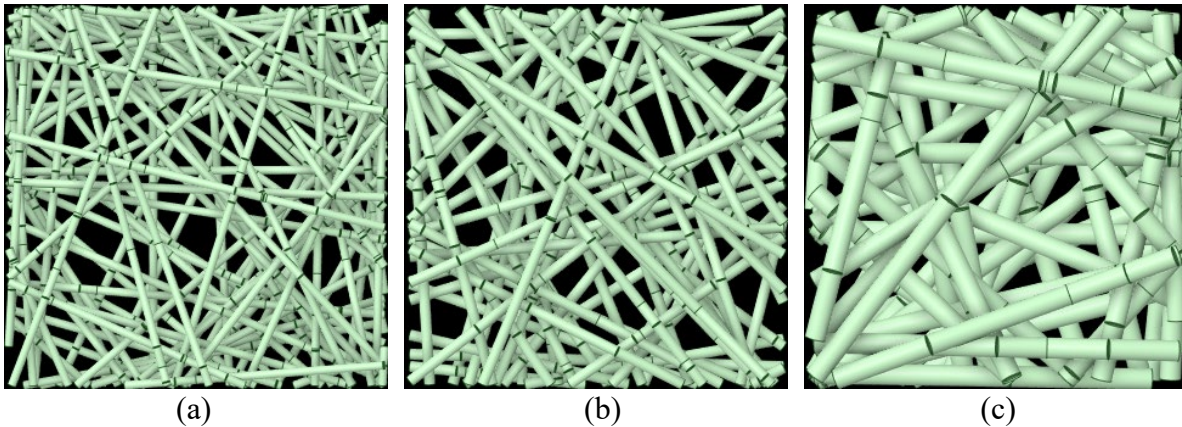


Figure 11. Images of first three of ten thousand digital twins.

Table V. Collection of 10,000 Images with Calculated Efficiency and Air Flow Resistance

Filter #	Fiber Flexibility (max slope)	Fiber Diameter ( $d_f$ ) ( $\mu\text{m}$ )	Face Coverage (FC)	Thickness ( $t$ ) ( $\mu\text{m}$ )	Solidity ( $\alpha$ ) (%)	Efficiency ( $E_f$ ) (%)	Air Flow Resistance ( $\Delta P$ ) (Pa)
1(a)	0.15	0.2918	1.3007	4.066	9.726	81.94	44.19
2(b)	0.15	0.2226	1.2886	3.479	8.891	88.88	56.11
3(c)	0.15	0.5795	1.2281	9.007	14.645	83.26	51.27
...	...	...	...	...	...	...	...
10000	0.15	0.4080	1.2454	3.590	11.23	61.29	25.39

The CNN was created using Tensorflow, Keras, and Python Imaging Library (PIL) on a Jupyter Notebook. Images were inserted into the CNN with input shape of  $64 \times 64$  pixels. After training the sequential CNN model through ten epochs, three images that were not included in the

training set were used for testing. Table VI shows the resulting accuracy of the CNN predictive model in determining air filter efficiency and air flow resistance of digital twin images. The results indicate an accuracy between 90% and 95% for predicting filtration efficiency and an accuracy between 80% and 95% for pressure drop.

Table VI. Results from Testing the CNN Predictive Model

Filter #	Efficiency ( $E_F$ ) (%)			Air Flow Resistance ( $\Delta P$ )		
	Predicted (%)	Actual (%)	Accuracy (%)	Predicted (Pa)	Actual (Pa)	Accuracy (%)
10,001	57.96	64.10	90.41	25.55	27.88	91.63
10,002	74.65	78.64	94.92	37.88	43.29	87.49
10,003	77.66	84.04	92.41	38.03	47.80	79.56

## CONCLUSION

The development of effective digital twin geometry creates a linkage between experimental, analytical, and computational modeling of air filter media. The digital twin algorithm described within this paper can be improved through incorporation of fiber curvature and non-circular fiber profiles into the geometry to more closely replicate actual air filter media. Furthermore, the computational model using Ansys Fluent can be improved by tuning the CFD parameters so that results from the computational model more closely align with results from the analytical model. Additional effort is required to correlate the analytical and computational results of the digital twin geometry with experimental results of real air filter media. The CNN model can be improved by increasing the image resolution, tuning the convolutional network with Keras Tuner, and training progressive stages of particulate loading. Additional effort is required to correlate the machine learning model with SEM imagery of real filter media.

## REFERENCES

1. Barnette, S., and G. Smith. 2003. "History of the Development of Air Cleaning Technology in the Nuclear Industry." *Nuclear Air Cleaning Handbook*. Accessed January 12, 2020. <https://www.standards.doe.gov/standards-documents/1100/1169-bhdbk-2003-ch1>.
2. First, M. 1998. "Hepa Filters." *Journal of the American Biological Safety Association*. Accessed March 3, 2022. <https://www.liebertpub.com/doi/10.1177/109135059800300111>.
3. Bergman, W., and S. Sawyer. 1988. "Development of a High-Efficiency, High-Performance Air Filter Medium." Presented at the 20th DOE/NRC Nuclear Air Cleaning Conference (August). Boston, MA. <https://www.osti.gov/servlets/purl/6946060>.
4. Bergman, W., G. Larsen, R. Lopez, K. Wilson, C. Witherell, and M. McGregor. 1996. "Further Development of the Cleanable Steel HEPA Filter, Cost/Benefit Analysis, and Comparison with Competing Technologies." United States: 37. <https://www.osti.gov/servlets/purl/325071>
5. Mitchell, M. A., W. Bergman, J. Haslam, E. P. Brown, S. Sawyer, R. Beaulieu, P. Althouse, and A. Meike. 2012. "Ceramic HEPA Filter Program." Presented at the International Society for Nuclear Air Treatment Technologies 32nd Nuclear Air Cleaning Conference. Denver, CO (May). <https://www.osti.gov/servlets/purl/1043641/>.

6. Haslam, J. J., and M. A. Mitchell. 2013. "Ceramic Filter with Nanofibers," US 2013/0048579 A1 (February 28).
7. Adamson, D. J. 1999. "Experimental Investigation of In Situ Cleanable HEPA Filters." U.S. Department of Energy (January). <https://www.osti.gov/servlets/purl/4852>.
8. Schemmel, A. 2017. "Evaluation of the ICET Test Stand to Assess the Performance of a Range of Ceramic Media Filter Elements in Support of ASME AG-1 Subsection FO." LLNL-TR-731529 (April). Livermore, CA: Lawrence Livermore National Lab. doi: 10.2172/1367985.
9. Cho, H., and C. A. Waggoner. 2016. "Effect of Elevated Temperature and Humidity on Air Flow for HEPA Filter Testing." Presented at the 34th Nuclear Air Cleaning Conference, San Antonio, TX (June). Accessed May 22, 2022. <http://isnatt.org/Conferences/34/Final%20Papers/23.%20Cho.pdf>.
10. Berry, G. N., H. Cho, and C. A. Waggoner. 2020. "Prediction for Pressure Differential Across HEPA Filter Media Based on Media Characteristics and Particle Size Distribution." INIS-US-21-WM-20-P20600. WM Symposia, Inc. (July). Accessed May 22, 2022. <https://www.osti.gov/biblio/23030268>.
11. Davies, C. N. 1973. *Air Filtration*. New York: Academic Press.
12. Hinds, W. C. 1999. *Aerosol Technology: Properties, Behavior, and Measurement of Airborne Particles*, 2nd ed. New York: Wiley.
13. Brown, R. C. 1993. *Air Filtration : An Integrated Approach to the Theory and Applications of Fibrous Filters*. New York: Pergamon Press.
14. Beckman, I. P., G. Berry, H. Cho, and G. Riveros. 2021. "Digital Twin Geometry for Fibrous Air Filtration Media." *Fibers* 9 (12): 84. doi: 10.3390/fib9120084.
15. American Society of Mechanical Engineers. 2020. "Code on Nuclear Air and Gas Treatment ASME AG-1-2019." ASME (January 17).